1

HW-37406

Radiation Effects on Reactor Materials (M-3679, 16th Ed.)

This document consists of 46 pages. Copy No. 102 of 166 copies. Series A

AEC RESEARCH AND DEVELOPMENT REPORT

THERMAL ANNEALING KINETICS OF INTERLAYER SPACING DAMAGE IN IRRADIATED GRAPHITE

By

R. E. Nightingale

Graphite and Materials Development Unit
Pile Materials Sub-Section

June 21, 1955

HANFORD ATOMIC PRODUCTS OPERATION
RICHLAND, WASHINGTON

Operated for the Atomic Energy Commission by the General Electric Company under Contract #W-31-109-Eng-52

RESTRICTED DATA

This document contains Restricted Data as defined in the Atomic Energy Act of 1954. Its transmittal or the disclosure of its contents in any manner to an unauthorized person is prohibited.

Route To:	Payroll No.	Location	Signature	Date

DISCLAIMER

INTERNAL DISTRIBUTION

Copy Number	
1	J. M. Atwood
2	L. P. Bupp
3	J. J. Cadwell
4	D. H. Curtiss
5	R. L. Dickeman
6	G. C. Fullmer
7	O. H. Greager
8	A. B. Greninger
9	M. Lewis
10	L. H. McEwen
11	R. E. Nightingale
12	W. J. Ozeroff
13	H. M. Parker - D. W. Pearce
14	P. H. Reinker
15	O. C. Schroeder
16	N. G. Wittenbrock
17	W. K. Woods - P. F. Gast
18	300 Files
19	Yellow File

EXTERNAL DISTRIBUTION

Copy Number	
20	AF Plant Representative, Wood-Ridge
21	Alco Products, Inc.
22	ANP Project Office, Fort Worth
23 - 28	Argonne National Laboratory
29	Armed Forces Special Weapons Project (Sandia)
30	Armed Forces Special Weapons Project, Washington
31	Army Chemical Center
32 - 35	Atomic Energy Commission, Washington
36	Battelle Memorial Institute
37 - 40	Bettis Plant (WAPD)
41 - 43	Brookhaven National Laboratory
44	Bureau of Ships
45 - 52	Carbide and Carbon Chemicals Company (ORNL)
53	Chicago Patent Group
54	Directorate of Research (WADC)
55 - 58	duPont Company, Augusta
59	Duquesne Light Company

EXTERNAL DISTRIBUTION (contd.)

Copy Number	
60	Engineer Research and Development Laboratories
61 - 63	General Electric Company (ANPD)
64	Hanford Operations Office
65 - 66	Headquarters, Air Force Special Weapons Center
67	Iowa State College
68 - 71	Knolls Atomic Power Laboratory
72 - 73	Los Alamos Scientific Laboratory
74	Materials Laboratory (WADC)
75	Mound Laboratory
76	National Advisory Committee for Aeronautics, Cleveland
77	Naval Research Laboratory
78	New York Operations Office
79 - 81	North American Aviation, Inc.
82	Nuclear Development Associates, Inc.
83	Nuclear Metals, Inc.
84	Patent Branch, Washington
85 - 88	Phillips Petroleum Company (NRTS)
89	Powerplant Laboratory (WADC)
90	Pratt and Whitney Aircraft Division (Fox Project)
91	Princeton University
92	Sylvania Electric Products, Inc.
93	USAF Project RAND
94	U. S. Naval Postgraduate School
95	U. S. Naval Radiological Defense Laboratory
96 - 97	University of California Radiation Laboratory, Berkeley
98 - 99	University of California Radiation Laboratory, Livermore
100	Vitro Engineering Division
101	Walter Kidde Nuclear Laboratories, Inc.
102 - 166	Technical Information Service, Oak Ridge

TABLE OF CONTENTS

LIST OF FIGURES AND TABLES

THERMAL ANNEALING KINETICS OF INTERLAYER SPACING DAMAGE IN IRRADIATED GRAPHITE

I. INTRODUCTION

Changes in properties of a graphite moderator in a nuclear reactor are effected by the very energetic particles produced by the fission process. It is vital to the operation of the reactors to know how, and to what extent, these changes have occurred. Furthermore, an understanding of the radiation damage process is necessary to predict further changes in the present graphite reactors and would be most helpful in choosing the best type of graphite for future reactors.

A rather detailed description of the microcrystalline structure of irradiated graphite is now available.[1] It is well known that when graphite is bombarded with energetic particles carbon atoms are displaced from their normal lattice positions resulting in a less well-ordered crystal with a certain amount of stored energy. A number of physical properties change as a result of this disordering process. Thermal and electrical conductivities decrease. Changes occur in the physical dimensions, in chemical activity, and in crystal lattice parameters. One of these changes which is easily detected and has been used to monitor radiation damage is an increase in the C_o spacing, the distance between alternate layers of carbon atoms in the crystal lattice. This C_o expansion is thought to be caused by carbon atoms or clusters of atoms displaced into interstitial positions forcing the planes apart. The C_o spacing damage may be annealed out by supplying sufficient thermal energy for interstitial atoms or other defects to return to stable lattice positions. An activation energy and release of stored energy will be associated with this process.

The nature of the thermal annealing process is not well understood. For example, one would like to know the mechanism by which a particular defect in the crystal lattice is annealed out, the rate at which this occurs, the activation energy required, net energy released, and the resultant

changes in physical properties. The latter two items have been studied by observing the net effect of annealing an irradiated sample for a given period of time. The former require measurements on the rate of annealing.

Rate experiments have been conducted on changes in thermal conductivity[2, 3] electrical resistivity,[2, 6] thermoelectric power,[2] elastic modulus,[5, 6] and stored energy.[7] The results have been interpreted in a number of ways, including the following:

1. A first order process for annealing of the measured physical property and a distribution of activation energies.
2. A first order process with several discrete activation states.
3. Higher order process with discrete activation states.

Primak[8] has recently reviewed these possible interpretations. He concludes that annealing of radiation damage produced in graphite is most easily described by a quasi-continuous activation energy spectrum which may be treated mathematically as a continuum.

The primary objective of this work is to add to the understanding of irradiated graphite. This report describes an experimental technique whereby changes in crystal lattice parameter may be studied as a function of time at constant temperature. The results given here are limited to changes in the C_o spacing for a typical sample of irradiated graphite in the temperature range 100 to 750 C.

II. SUMMARY AND CONCLUSIONS

A method has been developed to determine isothermal rates of annealing of radiation damage to the interlayer distance in graphite. Results are given for a sample with a cooled test hole exposure of 556 MD/CT in a Hanford reactor. Annealing was carried out at several constant temperatures in the range 100 C to 750 C resulting in a decrease in the C_o lattice parameter from 6.969 Å to 6.787 Å.

The data do not permit a determination of the kinetic order governing the annealing processes. The initial distribution of activation energy states was determined by the Vand method developed for first order processes. The effect of a different order upon the results derived from the Vand method is to decrease the resolution of any peaks in the activation energy spectrum. For the sample studied a sharp peak was found at 33 kcal/gm-atom and a broader maximum beyond the experimental range of this study at greater than 80 kcal/gm-atom.

Studies of samples irradiated under different conditions of flux and temperature should add to the understanding of radiation damage to graphite and provide a useful means of monitoring damage to a graphite moderator.

III. EXPERIMENTAL

The information sought in these experiments was the rate of change of C_o spacing as a function of time at a known constant temperature. Graphite samples were mounted in an insulating holder in a Norelco 180° X-ray diffractometer. CuK X-rays of 1.54 Å were obtained using Ni-Co monochromatizing Ross filters. An optical furnace and temperature control system were constructed to heat the sample to a constant temperature.

Graphite Samples

All data in this report were obtained from a sample of TS-GBF graphite exposed in cooled test hole facilities in the Hanford Piles. An exposure of 556 MD/CT (±10%) was accumulated by the sample at approximately 30°C, resulting in an increase in the C_o spacing of from 6.738 Å to 6.969 Å. Samples were introduced into the pile in the form of small cylinders 4" long and 0.43" in diameter. Following exposure they were machined to thin disks 1/8" thick. The machining was done at a sufficiently slow rate to produce a negligible temperature rise in the sample. A small hole was drilled in each graphite disk to accommodate the thermocouple. The method of mounting the sample is illustrated in Figure 1. Sample holders were machined from 1/8" lavite and the graphite disks were held

in place by tightly packed magnesium oxide. With this arrangement only a small amount of heat was conducted away from the sample through the holder. At the highest temperature used, there was a definite indication that the magnesium oxide had reacted with the graphite, suggesting that for temperature over 1000 C another packing material would be necessary. In later runs, Thermax was substituted for magnesium oxide and worked very well. In a few cases, the graphite disk lifted out of the position in the holder, probably due to sudden thermal shock. This could be observed visually and was also evidenced by a sudden change in the diffraction angle of the peak. These samples were discarded and were not used in subsequent calculations.

Thermocouples were constructed of 30 gauge chromel-alumel wire. In the early low temperature measurements, these were silver soldered, but because runs at temperatures greater than the melting point of silver are planned, an arc welding method was tried and was found to be very satisfactory. A strong weld was obtained with a DC rectifier unit at about 60 volts. One rectifier lead was firmly attached to a small cylinder of graphite. The thermocouple wires were wound together tightly, cut off, leaving about two turns, and attached to the other rectifier lead. The junction was touched to the graphite once or twice in an inert atmosphere of helium resulting in a small bead at the junction of the wires.

Optical Furnace

Figure 2 shows the arrangement of the optical furnace used to heat the sample. Power was supplied from the control circuit to a 750 watt T-12 projection lamp which was cooled by drawing air through a surrounding pyrex envelope. A spherical mirror was used to focus the lamp filament on to the sample. With the optical aperture of this system (f. 42) temperatures in excess of 1000 C could be obtained using approximately a 1:1 magnification of the filament.

It was necessary to surround the sample with an inert atmosphere during the high temperature (> 400 C) runs to prevent oxidation. This was most easily accomplished by enclosing the entire working top of the X-ray apparatus including the optical furnace in a plastic bag and flushing this volume with an inert gas. Helium and nitrogen and a combination of the two were tried. Two difficulties were experienced when helium was used. With a 100 per cent helium atmosphere at slightly greater than atmospheric pressure, the X-ray machine would consistently overload and shut off. This was apparently due to corona discharge from the high tension terminal of the Geiger tube. By diluting the helium with nitrogen, this difficulty was avoided. In this case, however, a constant mixture composition had to be maintained, since the X-ray absorption coefficients of the two gases are different enough to cause a considerable change in the intensity of the beam if the ratio of the He to N_2 should change. Operation was simplest with a 100 per cent nitrogen atmosphere and data in this report were obtained in this way. Oxidation of the samples was limited to a very slight roughening of the surface at the highest temperatures.

Temperature Recording and Control System

Sample temperatures were recorded on a Brown recording potentiometer with a 50 mv range. Although the temperature could not be accurately measured in this way, it was helpful to record the temperature while the sample was being brought rapidly to annealing temperature. Also, any gross deviations from the annealing temperature could be detected.

Figure 3 shows the circuit diagram of the temperature control system. A Leeds and Northrup K2 potentiometer was set to a voltage corresponding to the desired annealing temperature. A horizontal projection method was used with a Leeds and Northrup Type HS galvanometer. On either side of the null position of the galvanometer scale, a General Electric GL-929 photocell was clamped so as to intercept the light reflected by the swinging galvanometer mirror. The signal from each cell was amplified and used to actuate a relay and microswitch. When the temperature of the sample increased above that set on the potentiometer, the

galvanometer moved from the null position throwing a beam of light onto one of the photocells, adding a small resistance to the lamp circuit and causing the sample to cool slightly. In a similar way the other photocell, when actuated, switched the small resistance out of the circuit. The limits of the galvanometer swing determined the temperature variation in the sample and could be changed by adjusting either the distance between the photocells or the small resistance. A distance of 6 cm between photocells and a 0.4 ohm resistance worked satisfactorily and gave an estimated temperature variation in the sample of ± 0.25 C.

Experimental Procedure

A traverse of the C_o peak (002 reflection) was made of the sample at 25 C prior to an annealing run. The annealing temperature was chosen and set on the potentiometer. An estimate was made of the peak shift expected due to the temperature increase alone, and the goniometer was set on the high angle side of the peak so as to include the straight-line portion during the anneal. The temperature coefficient from the work of Nelson and Riley[9] on unirradiated graphite was used to estimate the peak shift due to the temperature.

$\Delta C_o \simeq 1.81 \times 10^{-4} \Delta T$, where ΔC_o is the shift in angstrom units from the 25 C value and $\Delta T = T\ (^oC) - 25$. This results in a shift in 2θ of,

$$\Delta(2\theta) \simeq 4\ (1.81 \times 10^{-4})\ \Delta T = 7.24 \times 10^{-4}\ \Delta T,$$

θ being the diffraction angle in the Bragg equation, $C_o = \frac{1.540}{\sin \theta}$.

Although the temperature coefficient assumed here is not the same as that found in highly damaged graphite, it is close enough to the true value to allow setting the goniometer properly prior to the annealing run. The method used for setting the goniometer for a run will be clear from Figure 4.

When the goniometer had been set to the proper angle, the sample was brought to annealing temperature manually by observing the temperature rise on the recorder. The control system was switched in at about the annealing temperature and fine adjustments were made to the voltage supplied to the projection lamp until it was in the range where the control system could maintain a constant temperature. A typical annealing curve is shown in Figure 4. Annealing temperatures were attained about 30 seconds after passing the previous annealing temperature. Annealing was continued until it was essentially complete at that temperature and a second traverse was made of the C_o peak, this time at the annealing temperature. Following this, a new temperature was chosen and this procedure was repeated mutatus mutandis on the same sample. Temperatures 25 to 100 C above the previous anneal were chosen so as most conveniently to follow the annealing rate and were determined by the total amount of the anneal expected in the temperature interval. The result of a typical annealing run is shown in Figure 4.

Rate Data

The information from runs such as given in Figure 4 has been reduced to a table giving the functions, $\Delta(t)$ and $\frac{d\,\Delta(t)}{dt}$ for each value of the time. They are defined as,

$\Delta(t) = \Delta_\infty - \Delta_t$

Δ_t = the shift after time, t, from the initial value of the 002 reflection peak in units of (2θ).

$\Delta_\infty = \Delta_t$ after the annealing is essentially complete at the annealing temperature, T_A.

t = time of anneal in minutes.

Figure 5 will illustrate the method used to reduce the X-ray charts to the desired quantities. The coordinates Z(t) and t are drawn on the chart.

$$Z(t) = \alpha \Delta_t = \alpha (\Delta_\infty - \Delta(t))$$

where α is the slope of the high angle side of the post-anneal peak. The recording pen may be thought of as moving up this peak as annealing proceeds.

$\Delta(t)$ and $Z(t)$ are related by,

$$\Delta(t) = \frac{1}{\alpha} (Z_\infty - Z(t))$$

and $$\frac{d\Delta(t)}{dt} = -\frac{1}{\alpha} \frac{dZ(t)}{dt} .$$

The choice of Z_o is somewhat arbitrary, but because the two lines intersect rather sharply at the time when T reaches T_A, a reasonable choice for Z_o is the intersection of these lines. It is estimated that the resulting uncertainty in t_o should be less than ± 0.2 minute. A greater uncertainty in t_o arises from the heating period, that is, the time required to bring the sample to T_A from the previous annealing temperature. This was about 0.5 minute in most runs, and of course some annealing was done during this time. However, the heating period was quite short compared to the half-life of the annealing process and so it has been assumed that annealing did not begin until T_A was reached.

Z_o may also be predicted from the C_o temperature expansion coefficient, assuming no annealing had taken place by the time T_A was reached. It agrees, within the rather large uncertainties involved, with the Z_o determined from the intersection of the two curves.

The slopes, $\frac{d\Delta(t)}{dt}$, were measured after drawing a smooth curve through the X-ray tracing. As the slope approaches zero, the uncertainties become large and this accounts for the large scatter in data when t is greater than about 30 minutes.

A quantity more fundamental than $\Delta(t)$ is the change in C_o spacing. Over the range of (2θ) studied here, the relation $C_o = \frac{178.04}{(2\theta)}$ may be used with an accuracy of ± 0.03 per cent in changing to C_o in angstrom units.

The use of $\Delta(t)$ and $\frac{d\Delta(t)}{dt}$ is, to a good approximation, equivalent to use of C_o and $\frac{d\,C_o}{dt}$. Tabulation of the exact values of the latter is more time consuming and so has not been done.

Annealing runs were carried out on nine disks machined from the same four inch cylinder. Most of the data reported comes from Sample 11 on which annealing was carried to 750 C. Annealing of the other samples was discontinued at 400 to 650 C, but the results of these are similar at comparable temperatures to the sample annealed to 750 C, so that results on Sample 11 are typical. Some pertinent experimental details are given in Table I. 11-1 was a 98.8 C run during which no annealing was observed. The rate data are presented in Table II starting with Run 11-2.

Temperature Coefficient of C_o Distance

A large change of the temperature coefficient of C_o distance with state of damage of the graphite sample would cause errors in the interpretation of the rate data since part of the change observed during the isothermal annealing runs would be due to a changing temperature coefficient and part to a true annealing of the damage. An experiment was designed to estimate the magnitude of this effect.

Δ_t may be divided into two parts,

$$\Delta_t = \Delta\,{}^{A}_{t} + B_t \cdot T_A$$

where, Δ_t is the total measured effect

${}^{A}_{t}$ is that part of Δ_t due only to annealing

$B_t\,T_A$ is that part of Δ_t resulting from a change of temperature coefficient with damage.

To estimate B_t, a graphite disk was taken from the same four-inch cylinder that was used for the rate experiments. This was annealed at some temperature, T_A, until the rate of removal of damage became very slow. The 002 peak was traversed at T_A, and at a series of temperatures

below T_A. The temperature was then increased, the sample was annealed at a higher T_A, and the measurements repeated.

Figure 6 shows the results of these runs. B_t, the slope of the straight lines for each annealing temperature is plotted against annealing temperature in Figure 7. There is a small, though significant change in B_t with state of damage of the graphite.

A large amount of annealing was done in Run 11-4, so this will be used as an example to estimate B_t T_A.

$$(\Delta_\infty - \Delta_o) = \Delta^A_\infty - \Delta^A_o + (B_\infty - B_o) \cdot T_A$$

$\Delta_\infty = 8.19 \times 10^{-3}$

Δ_o and $\Delta^A_o = 0$

$B_\infty \approx$ B after 200 C anneal.

$B_o \sim$ B after 150 C anneal.

$\Delta_\infty = \Delta^A_\infty + (8.14 - 8.10) \times 10^{-4} \times 200$

$819 \times 10^{-4} = \Delta^A_\infty + 8 \times 10^{-4}$

The effect due to a change of temperature coefficient is about one per cent of the total measured effect and will be neglected.

A similar type of calculation may be made for $\frac{d\Delta_t}{dt}$ if some relation is assumed between Δ_t and B_t. For a linear relation, $\frac{d\Delta^A_t}{dt}$ is less than one per cent of $\frac{d\Delta_t}{dt}$ at all times during the run. In subsequent calculations, it will be assumed that $\Delta^A_t = \Delta_t$ and $\frac{d\Delta^A_t}{dt} = \frac{d\Delta_t}{dt}$.

IV. DISCUSSION

Phenomenological Activation Energy

One of the first questions that arises in interpreting the rate data is this: Does the annealing process involve one, a few, or a whole distribution of activation energies? Dienes, and co-workers,[10] have published some work which can help to answer this question. This technique allows the determination of the activation energy without assumptions as to order of reaction or dependence of the physical property measured upon the number of processes occurring. If the order of the reaction is γ, and the process occurs by a single activation energy, then,

$$\frac{dn}{dt} = -kn^{\gamma}$$

where n is the number of some fundamental lattice distrubance. For $n = n_o$ at $t = o$, and $k = Ce^{-E/RT}$,

$$\frac{n_o^{1-\gamma} - n^{1-\gamma}}{C(1-\gamma)} = te^{-E/RT}.$$

The physical property studied, p, will be related in some way to n,

$$p = g(n)$$

and combining these equations,

$$\frac{h(p_o) - h(p)}{C(1-\gamma)} = te^{-E/RT}$$

where p_o is the value of p at $t = o$ and h is some unspecified function of p. By studying samples which are the same at $t = o$, and annealing to some given value of p, the left side of this equation will be a constant and independent of T.

$$te^{-E/RT} = \text{constant}$$

and $\ln t = \frac{E}{RT}$.

A plot of log t vs $\frac{1}{T}$ should give a straight line with slope equal to $\frac{E}{2.3R}$. A curved line implies that the process does not occur by a single activation energy. Figure 8 shows such a plot for a series of three runs. Prior to making these runs, each sample was annealed to 150 C until the rate of annealing was practically zero. Although only three points have been obtained, it is apparent that there is a definite curvature to each line. Further, the curvature is such that an activation energy calculated from the slope would be greater for the higher temperature runs. Average activation energies from each curve is the order of 40 kcal/g atom. It is not intended that much meaning be attached to this average value of 40 kcal activation energy, since curvature in each line is large. However, this plot does indicate that the annealing process does proceed by more than one activation energy.

Activation Energy Spectrum

The previous section indicates that any kinetic-treatment of the rate data must be complicated by allowing for more than one activation energy. Vand[11] has given a method of treating kinetic problems involving a distribution of activation energies. This was developed for a study of electrical resistance changes of metallic films evaporated in vacuum. More recently it has been applied by several workers[4, 5, 8] to thermal annealing of irradiated graphite. The essential steps of the Vand analysis will be repeated here to point out clearly the assumptions involved and to prepare a basis for a discussion of the theory.

The annealing of dislocations in the crystal lattice is assumed to follow the first order rate law,

$$\frac{d\,N(E,\,t)}{dt} = -\,k(E)\,N(E,\,t)$$

N (E, t) is the number of dislocations with activation energy, E, at time, t. k (E) is the first order rate constant for annealing dislocations of activation energy, E, and is given by,

$$k(E) = Ce^{-E/RT}$$

Integrating, $N(E, t) = N_o(E)\, e^{-k(E)\, t}$

For the case of annealing C_o damage,

$$\Delta(t) = \int_o^\infty N(E, t) \cdot \delta(E)\, dE = F_o(E)\, \phi(E, t)\, dE$$

where $\Delta(t) = \Delta_\infty - \Delta_t$

$\delta(E)$ = the contribution to $\Delta(t)$ from one dislocation requiring activation energy, E, to be annealed.

$F_o(E) \equiv N_o(E) \cdot \delta(E)$

$\phi(E, t) \equiv e^{-k(E)\, t}$

The function $\phi(E, t)$ is plotted in Figure 9 for three values of t. Values for the constants involved are representative of those involved in the C_o annealing data.

Vand approximated ϕ with the step function,

$\phi = 0 \quad E < E_o$.

$\phi = 1 \quad E > E_o$.

This is shown as a dotted line in Figure 9. E_o is the value of E at the inflection point of ϕ and is given by,

$$E_o = RT \ln Ct$$

From Figure 9 it is apparent that the shape of ϕ does not change appreciably with t.

With this approximation to ϕ,

$$\Delta(t) = \int_{E_o(t)}^\infty F_o(E)\, dE$$

and,

$$\frac{d\Delta(t)}{dt} = -F_o(E_o)\frac{dE_o(t)}{dt} = -\frac{F_o(E_o)RT}{t}$$

$$F_o(E_o) = -\frac{t}{RT}\cdot\frac{d\Delta(t)}{dt}$$

Thus it is possible to calculate the distribution function $F_o(E_o)$ for each value of t from the rate of change of $\Delta(t)$ with time. Also, E_o may be calculated for each value of t from the equation, $E_o = RT \ln Ct$. The plot of $F_o(E_o)$ vs E_o has been called the activation energy spectrum and is shown for Sample 11 in Figure 10. The dotted lines are drawn through the experimental points for each run. The full line is the envelope of the dotted lines and represents the state of the sample prior to annealing. The state of the sample following an anneal to, say, 350 C, is given approximately by following the dotted curve of the 425 C run to the full line and out to the end of the full line. The activation energy spectrum shows a sharp maximum at about 33 kcal/g atom. There also appears to be a broader maximum beyond the experimental range of this study at > 80 kcal/g atom.

The effect of the approximation to ϕ was shown by Vand to decrease the "resolution" of any sharp peaks in $F_o(E_o)$. For a process occurring with a single activation energy E*, the following is true.

$$\frac{F_o}{F_{o_{max}}} = y e^{1-y}$$

where

$$y = e^{(E_o - E^*)/RT}$$

Figure 11 is a plot of $\frac{F_o}{F_{o_{max}}}$ vs $(\frac{E_o - E^*}{RT})$. As a result of the approximation to ϕ,

SECRET

the true activation energy, E*, (which would be a straight vertical line in this case) has been smeared out and is represented as a band of energies as shown. The maximum of this band comes at $E_o = E^*$. The width of the band as measured by the distance from $E_o = E^*$ to the inflection points is 0.96 RT. Thus, as Vand and others have pointed out, a peak in the activation energy spectrum of width $\sim$2 RT may be interpreted as arising from a single activation energy. From these considerations the peak at 33 kcal in the curve of Figure 10 appears to arise from a very narrow band, approaching a discrete activation energy.

Although it is certain that a large peak exists at about 33 kcal, it is possible that the shape and size may be somewhat different from that shown in Figure 10. This is due to the relatively larger uncertainties in $F_o(E_o)$ as the slope of the annealing curve approaches zero for each of the runs. This is evidenced by the scatter in the points toward the end of each run. It is not serious except in region of the 33 kcal peak.

Activation energies of Figure 10 depend on the value chosen for C, the collisional constant. Values between 10^{10} sec^{-1} and 10^{14} sec^{-1} have been used, but most workers have chosen a value of about 10^{13} sec^{-1}. Energies in Figure 10 have been calculated with $C = 7.5 \times 10^{13}$ sec^{-1}. Vand defines C as,

$$C = 4nf$$

where n = number of dislocations necessary to initiate a reaction, and

f = maximum Debye frequency.

f was taken as 1.875×10^{13} sec^{-1}, based on some recent work on graphite[13] in which the specific heat was fitted by dividing the lattice vibrations into modes with atomic displacements perpendicular to the layer planes with a Debye temperature of 900°K, and modes with atomic displacements parallel to the planes with a Debye temperature of 2500°K. The Debye temperature

of the perpendicular modes was rather arbitrarily chosen as best representing collisional process and corresponds to a frequency of $f = 1.875 \times 10^{13}$ sec^{-1}. With n = 1,

$$C = 4 \times 1 \times 1.875 \times 10^{13} = 7.5 \times 10^{13} \text{ sec}^{-1}.$$

It is possible that C changes over the range of temperatures studied, but in view of the uncertainties involved, no attempt has been made to account for such variations. However, since E_o depends on the ln C, it is not too sensitive to the value taken for C. This is shown by,

$$E = E' + 2.3 \text{ RT log } \frac{C}{C'},$$

where E and E' are values calculated using C and C' respectively.

The spectrum of Figure 10 might be interpreted in three ways. The large value of $F_o(E_o) = N_o(E) \cdot \delta(E_o)$ at 33 kcal, for example, could arise from: (i) a large number of dislocations requiring an activation energy of 33 kcal/g-atom to return to stable lattice positions; (ii) relatively larger contributions to $\Delta(t)$ from dislocations with 33 kcal activation energy, or (iii) a significant contribution to $F_o(E_o)$ by both $N_o(E_o)$ and $\delta(E_o)$. There is no way at present to unequivocally choose between the (i), (ii), or (iii) since the dependence of $\delta(E)$ on E is unknown. However, other studies on irradiated graphite indicate that (i) may be a good choice.

In Figure 12, the stored energy spectrum of a sample of irradiated graphite has been reproduced from some work of J. C. Ballinger.[12] The similarity of the stored energy and activation energy curves is quite striking. Both show a sharp maximum corresponding to conveniently measurable rates at about 200 C with smaller and broader peaks at about 400 C and 550 C. The irradiation histories of the two samples are roughly comparable, the stored energy curve resulting from a sample exposed to 651 MD/CT in a cold test hole. It is very likely that the peaks in the stored energy spectrum result from relatively larger numbers of dislocations being annealed at the temperatures shown. This would require a large number of

dislocations in the same regions of the activation energy curve where maxima are observed. In this case interpretation (i) is a reasonable one.

The region of the activation energy spectrum between 40 and 75 kcal contains no intense maxima, suggesting that sections of it might be described by $F_o(E_o)$ = constant. It is of interest to see how well the Vand theory will predict values of $\Delta(t)$ in these regions. For a given annealing temperature,

$$\Delta(t') - \Delta t \simeq - F_o(E_o) \int_{E_o(t)}^{E_o(t')} dE_o = - RT\, F_o(E_o) \int_t^{t'} \frac{dt}{t}$$

$$= - RT\, F_o(E_o) \ln \frac{t'}{t}$$

In terms of Z (t),

$$\log t = \log t' + \frac{Z(t) - Z(t')}{2.3\, RT\, \alpha\, F_o(E_o)}$$

Log t vs Z(t) has been plotted in Figures 13 and 14 for Runs 11-6 and 11-7. Average values of $F_o(E_o)$ from Figure 10 are used in the calculations. Experimental values of Z(t) are shown for comparison. The agreement is good over the region where $F_o(E_o)$ is constant.

The total amount of annealing done on Sample 11 in units of (2 θ) should agree with that calculated from the Vand method. This may be checked by the equation,

$$\Delta(t_1) - \Delta(t_2) \simeq \int_{E_o(t_1)}^{E_o(t_2)} F_o(E_o)\, dE_o$$

The right side of the equation was obtained by graphical integration and is equal to the area under the activation energy curve from 25 kcal to 80 kcal.

$$\int_{25}^{80} F_o(E_o)\, dE_o = 0.76^o$$

$\Delta(t) - \Delta(t_2)$ may be calculated from the 25 C C_o peak positions.

$$\Delta(t_1) - \Delta(t_2) = (2\theta)_2 - (2\theta)_1$$
$$= 26.23 - 25.53 = 0.70^o.$$

The two values disagree by less than 9 per cent. This is as good as can be expected considering the uncertainties in drawing in the details of the activation energy curve.

It is of interest to compare Figure 10 with similar curves for irradiated graphite where other physical properties have been used to measure the radiation damage. Both Seifert[4] and Neubert[5] have observed a peak in the 30 to 35 kcal region using electrical resistance as a measure of damage. Irradiation exposure of the samples was only 10 L units, which is roughly equivalent to 7 MD/CT Hanford exposure. Neubert also found a small broad peak at 31 kcal and a larger broad peak at 42 kcal from rate studies of changes in elastic modulus with samples of 10 L units exposure at 35 C. A value of 1.1×10^{13} sec^{-1} was taken for the collisional constant. Primak[8] analyzed some tempering experiments on stored energy release rates for samples with a large Hanford exposure at about 150 C. The 30 kcal peak was absent. Using $C = 10^{14}$ sec, the resulting activation energy spectrum was a slowly increasing curve between 57 kcal and 76 kcal. All of these features are compatible with the activation energy curve of Figure 10 if the same value for C is used.

Kinetic Order of the Annealing Process

No attempt will be made to determine the order of the annealing process over the entire range of temperatures studied. The problem is complicated by the fact that the activation energy for the process is not constant. This means that there are several different kinds of processes occurring concurrently, in different proportions, possibly with different kinetic orders. Thus, the order of reaction loses much of the significance

it has in gas phase reactions or simple solid-solid reactions.

It is possible to discuss the order of the process resulting in the relatively sharp maximum in the activation energy spectrum at 33 kcal. The half-intensity band width is about 5 kcal. If this resulted from a single activation energy at 33 kcal, the band should have a width of about 2 kcal due to the limited resolution of the Vand method. In the approximation that only one kind of lattice defect is being annealed,

$$\Delta(t) = \delta N(t)$$

and for a first order process,

$$\ln \frac{\Delta(t)}{\Delta_\infty} = -kt,$$

or for a second order process,

$$\frac{1}{\Delta(t)} - \frac{1}{\Delta_\infty} = kt.$$

These two equations have been used to test the data from Runs 11-2 and 11-3 which contribute most heavily to the 33 kcal peak. (Figure 15 and 16). Upon casual inspection, it would appear that the data are best fitted by a second order law. Run 11-2 shows a significant deviation from a straight line for times less than 4 minutes, but after that the data lie on a good straight line. Points from Run 11-3 lie fairly close to a straight line throughout the course of the reaction. Both first order plots show lines continuously decreasing in curvature as the reaction proceeds. When drawing conclusions from these plots, it should be remembered that the Vand analysis results in a peak about 2 1/2 times as broad as would be expected if the process occurred by a single activation energy, indicating that even this relatively sharp peak at 33 kcal does not arise from a single first order process. Thus the first order plot is qualitatively what would be expected. The line should have a positive curvature giving a smaller

"instantaneous" first order rate constant as the reaction proceeds. Conversely, it could be reasoned that the reaction is second order and the assumption of first order kinetics in the Vand analysis has decreased the resolution to the extent that the peak has been broadened to 5 kcal at half-intensity. It must be concluded that no decision between these two possibilities can be made from the existing data. This does not alter the conclusions concerning the activation energy spectrum, but the possibility exists that the process is not first order over the complete range of temperatures, and this would result in poorer resolution than is predicted from first order considerations.

Other workers have attempted to determine the order the process in the 200C annealing region. Kinetic orders from less than one[8] to six[14] have been suggested. To date there is no work which has given a definite answer to this question. Determination of the order at higher annealing temperatures will be more difficult because of the broad distribution of activation energies.

V. ACKNOWLEDGEMENTS

The author is grateful to Mr. J. C. Ballinger who designed and built the temperature control apparatus. He also would like to acknowledge the many helpful discussions with other members of the Graphite and Materials Development Unit.

R. E. Nightingale

REN:ag

R. E. Nightingale

BIBLIOGRAPHY

1. J. R. Townsend, HW-24982, May 10, 1952.
2. A. S. Hook, NAA-SR-193, October 27, 1952.
3. A. S. Hook, NAA-SR-119, January 24, 1952.
4. R. L. Seifert, ANL-4196, September 13, 1948.
5. T. J. Neubert, ANL-4369, November 18, 1948.
6. T. J. Neubert, ANL-4477, July 7, 1950.
7. J. C. Ballinger, Reactor Sci. Technology, 3, 55, (1953).
8. W. Primak, Nuclear Sci. Technology, 1, 143, (1955).
9. J. B. Nelson and D. P. Riley, Proc. Phys. Soc. (London), 57, 477, 486, (1945).
10. W. E. Parkins, G. J. Dienes and F. W. Brown, J. Appl. Phys., 22, 1012, (1951).
    G. J. Dienes, J. Appl. Phys., 22, 1020, (1951).
11. V. Vand, Proc. Roy. Soc., (London), 55, 222, (1943).
12. J. C. Ballinger, HW-24692, June 17, 1952.
13. J. Krumhansl and H. Brooks, J. Chem. Phys., 21, 1663, (1953).
14. D. Bowen, NAA-SR-41, August 4, 1950.

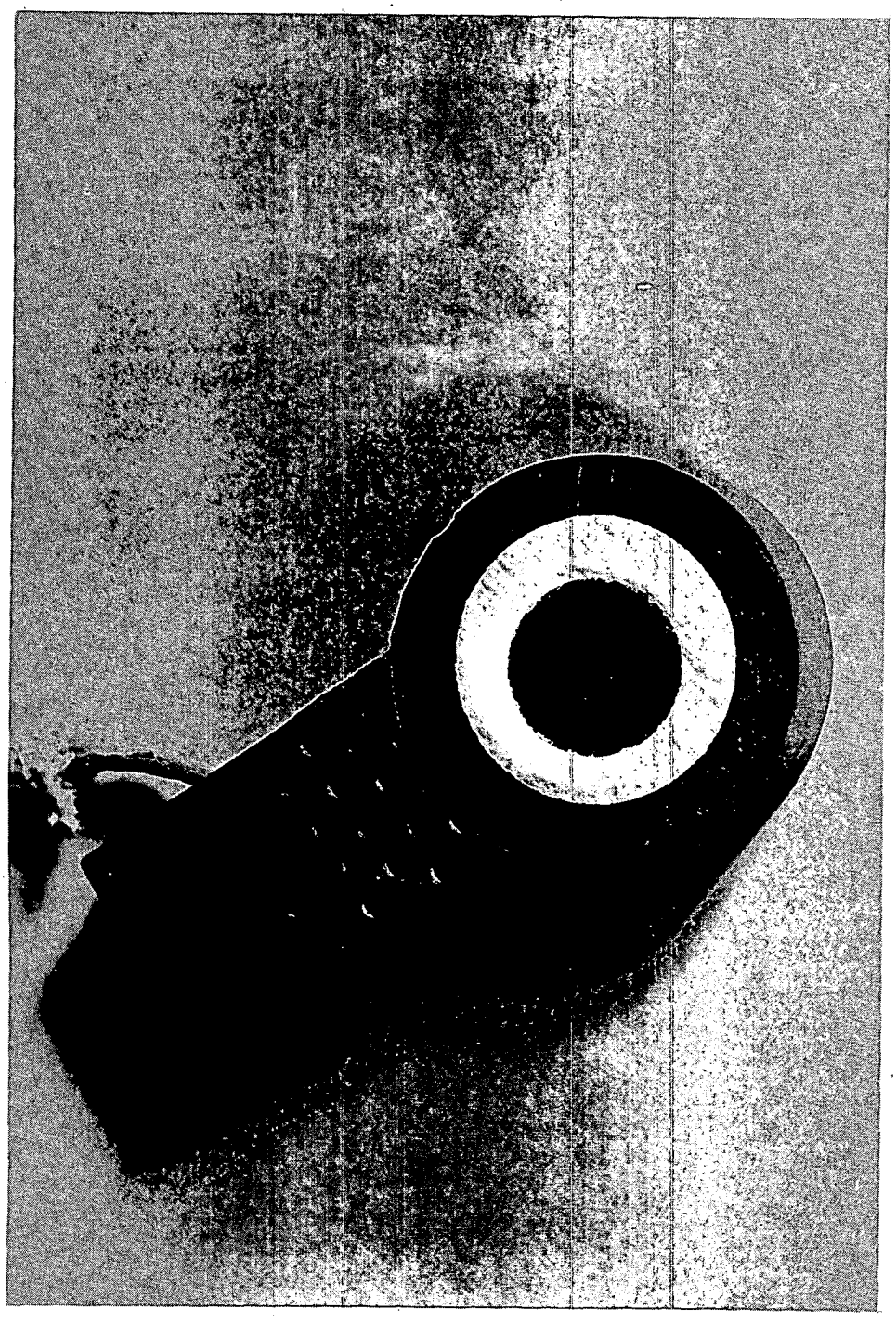

FIGURE 1
MOUNTING OF GRAPHITE SAMPLES

AEC-GE RICHLAND, WN.

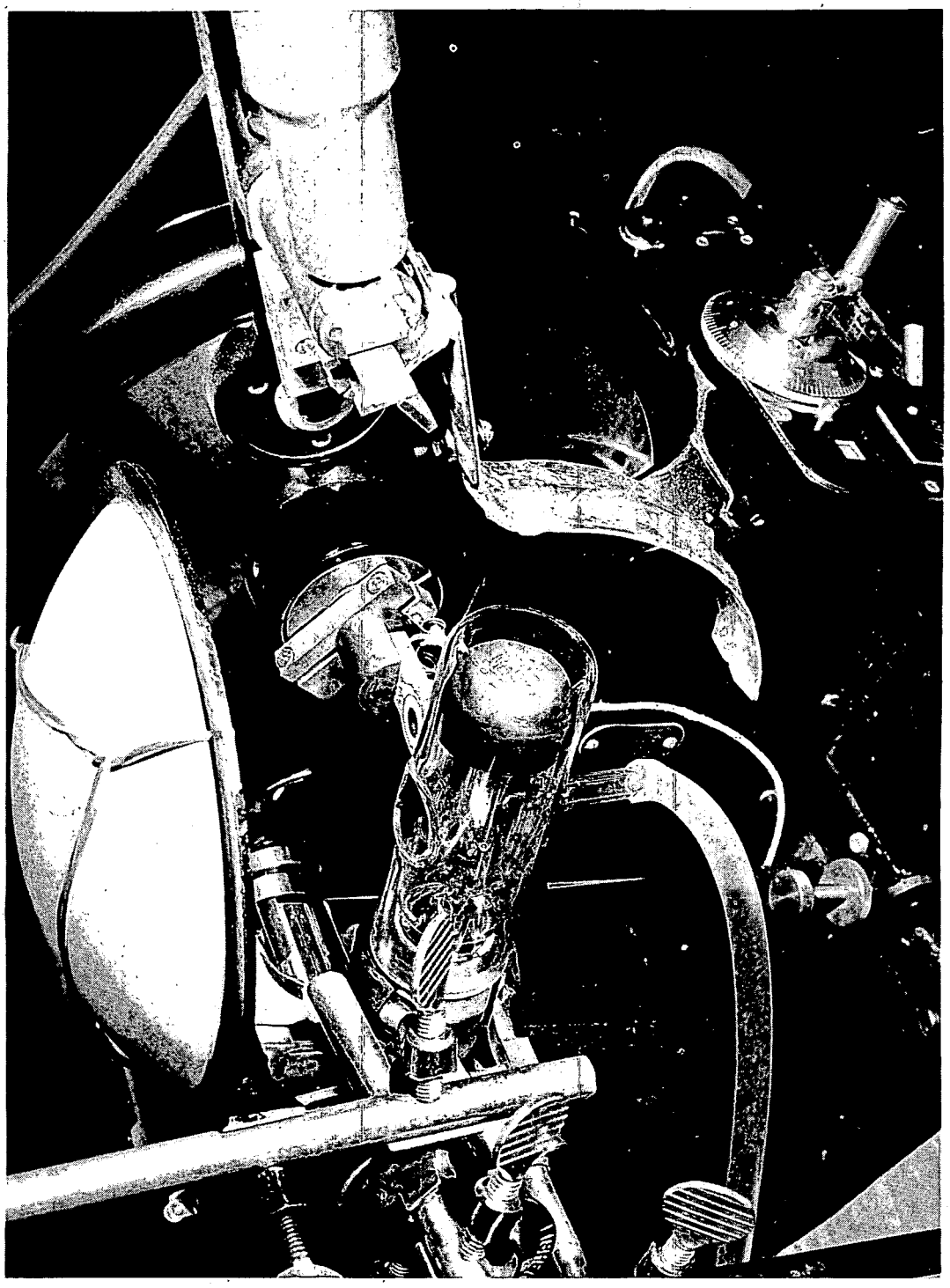

FIGURE 2
OPTICAL FURNACE

AEC-GE RICHLAND, WN.

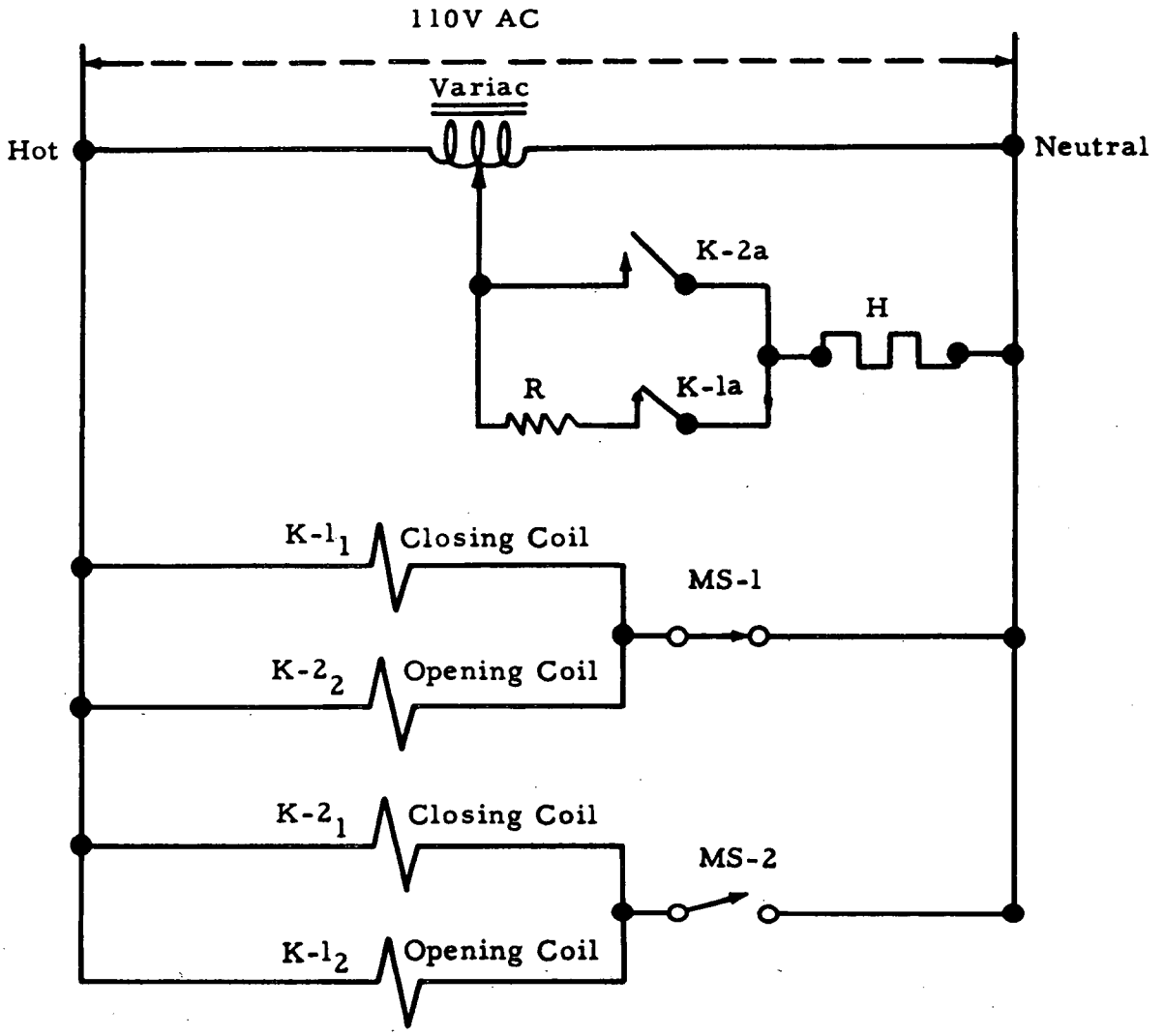

R 0.4 Ω Resistance
H 750 W 120V Projection Lamp
K-1a Relay 1 Contact
K-1$_1$ Relay 1 Closing Coil
K-1$_2$ Relay 1 Opening Coil
MS-1 Microswitch 1

FIGURE 3
TEMPERATURE CONTROL CIRCUIT

AEC-GE RICHLAND, WASH.

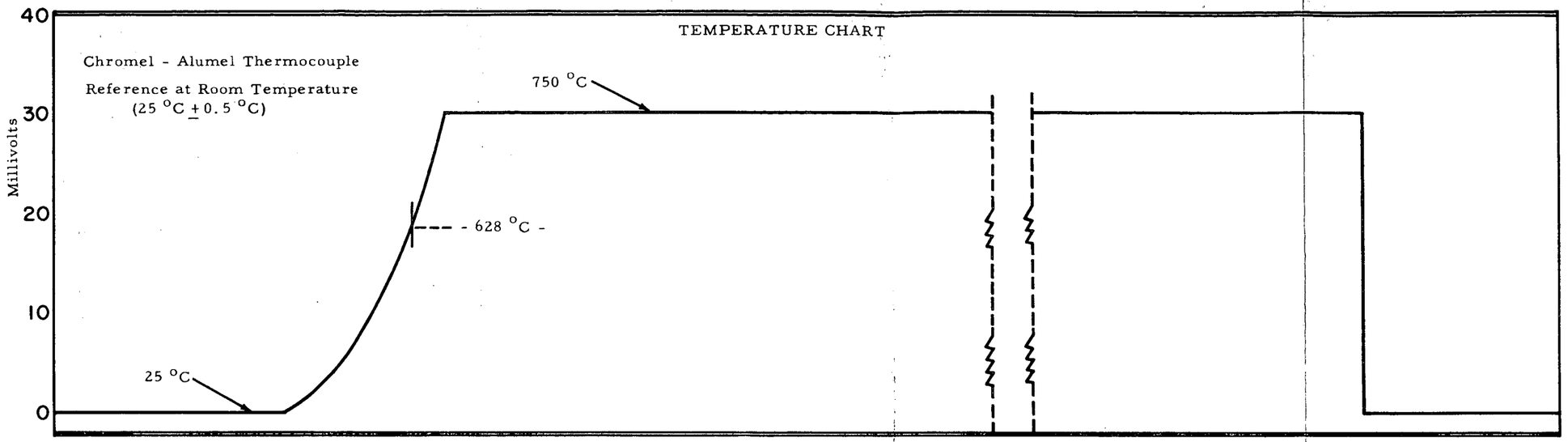

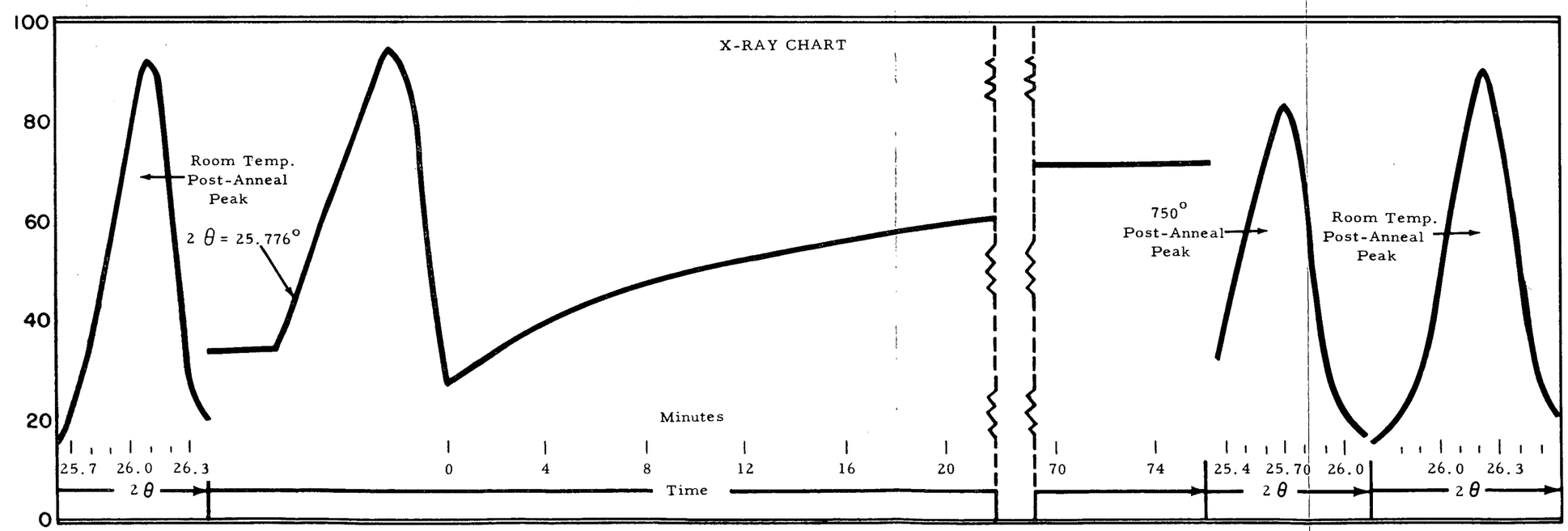

FIGURE 4
RESULTS OF A TYPICAL ANNEALING RUN

AEC-GE RICHLAND, WN.

32

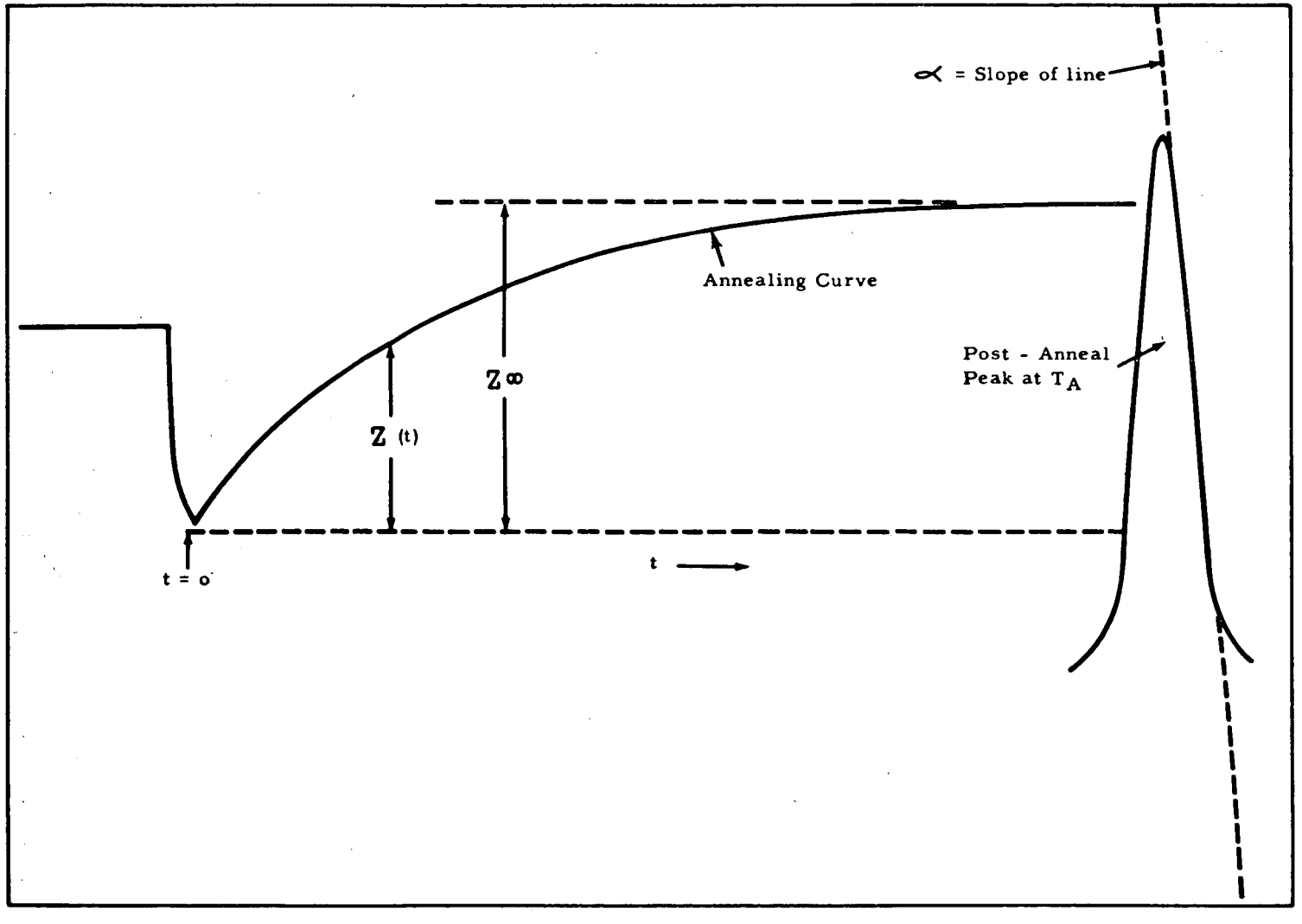

FIGURE 5
REDUCTION OF CHARTS TO RATE DATA

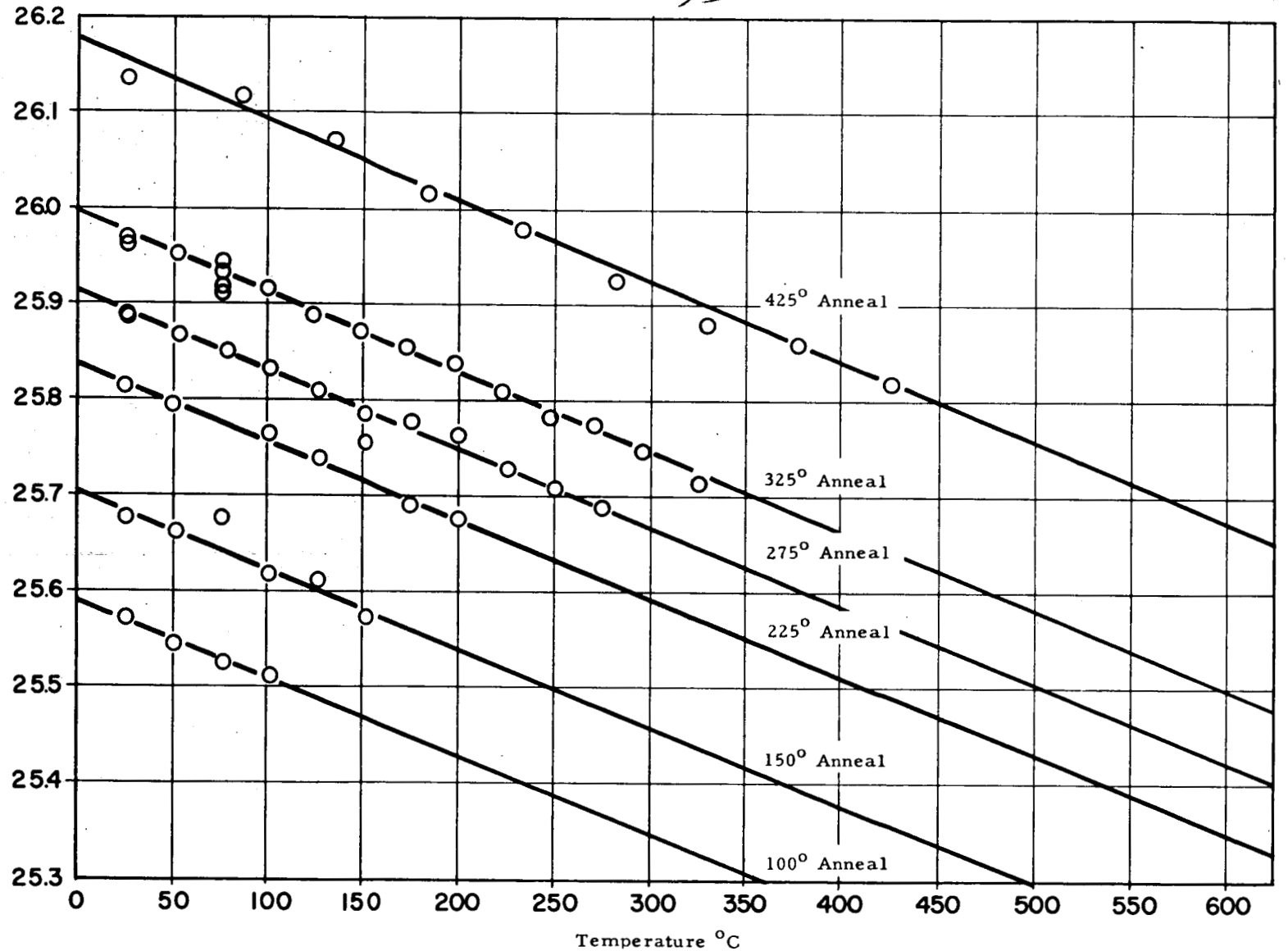

FIGURE 6
TEMPERATURE COEFFICIENT OF THE 002 PEAK

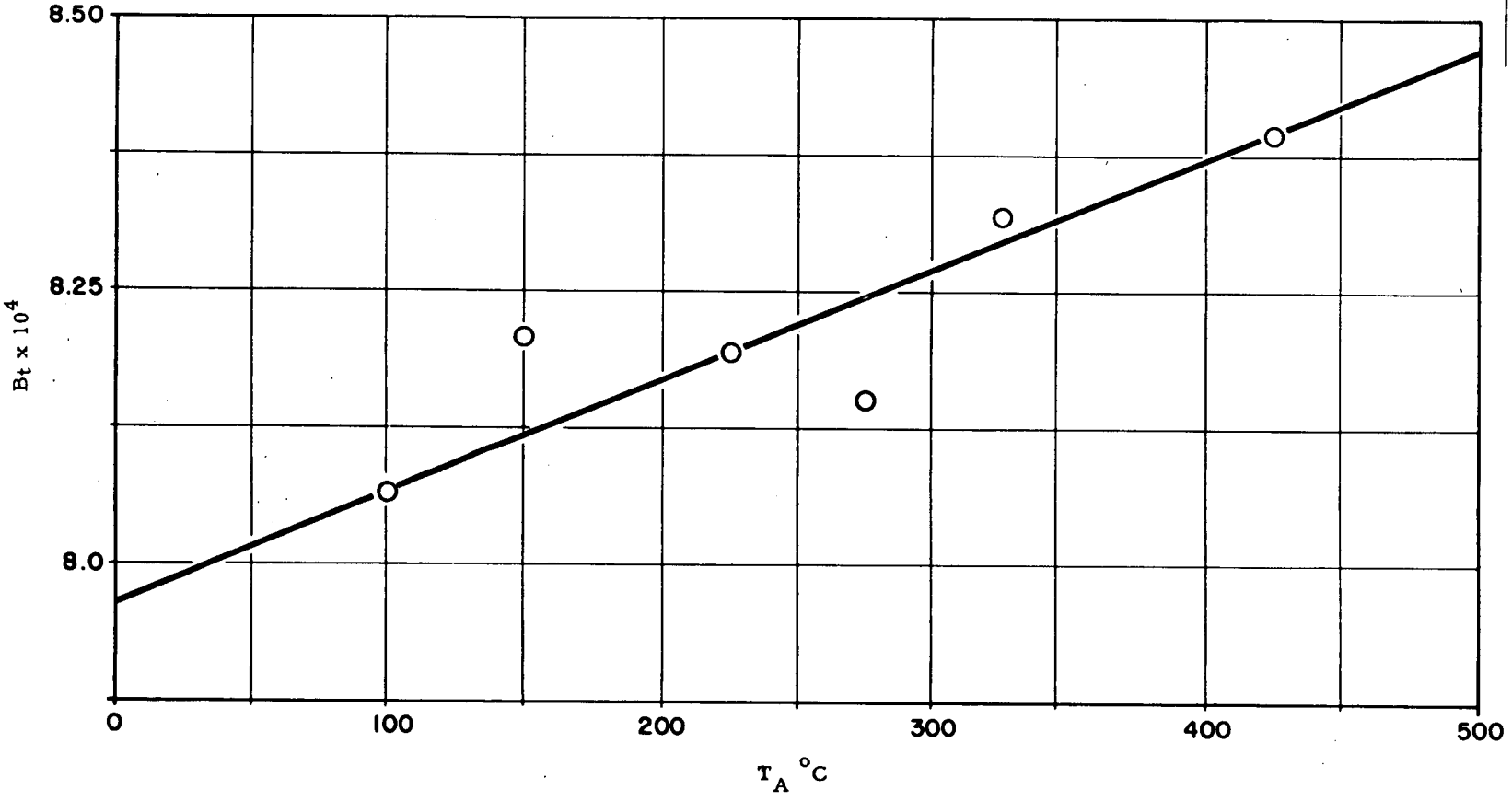

FIGURE 7
B_t vs ANNEALING TEMPERATURE

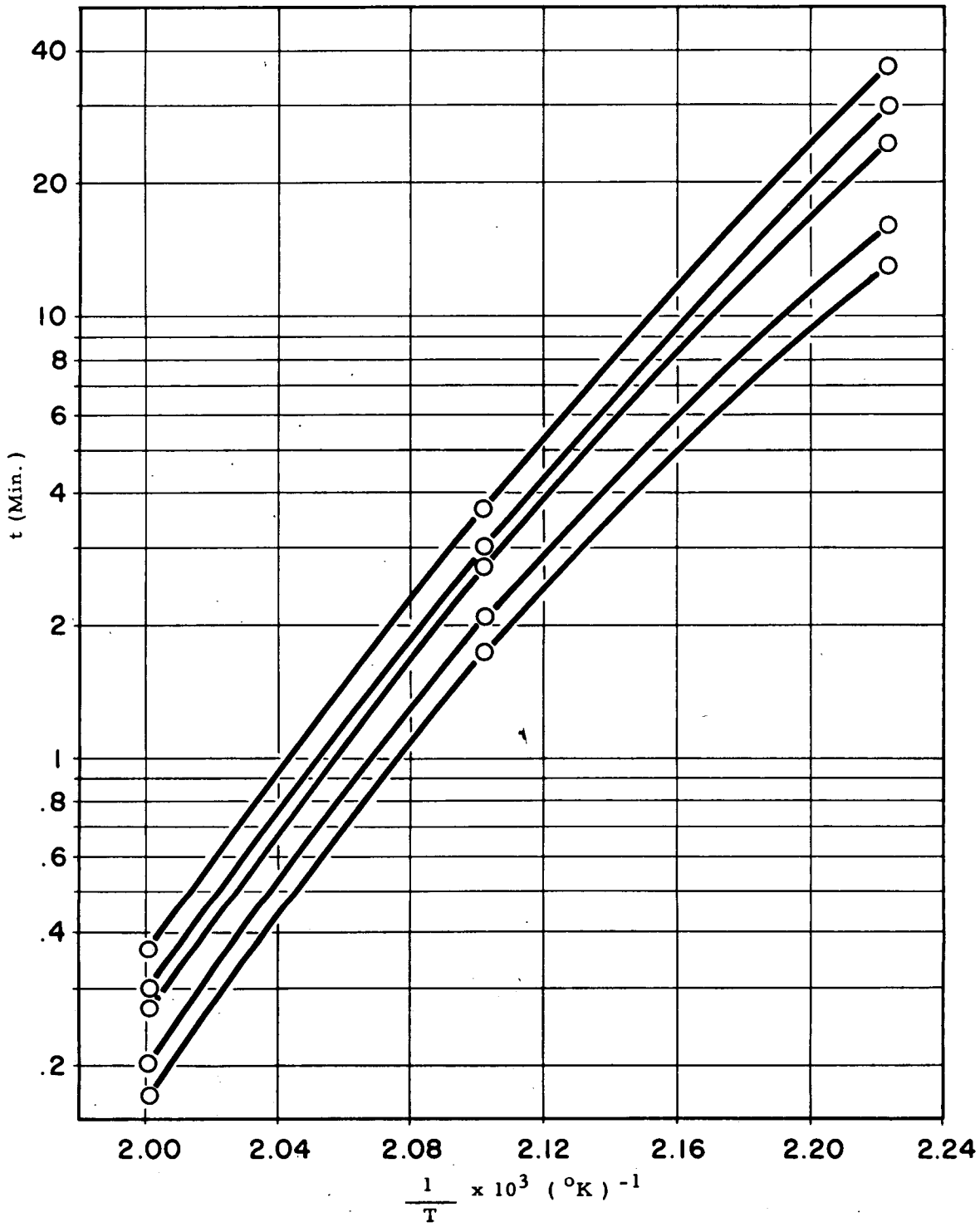

FIGURE 8
PHENOMENOLOGICAL ACTIVATION ENERGY PLOT

AEC-GE RICHLAND, WN.

36

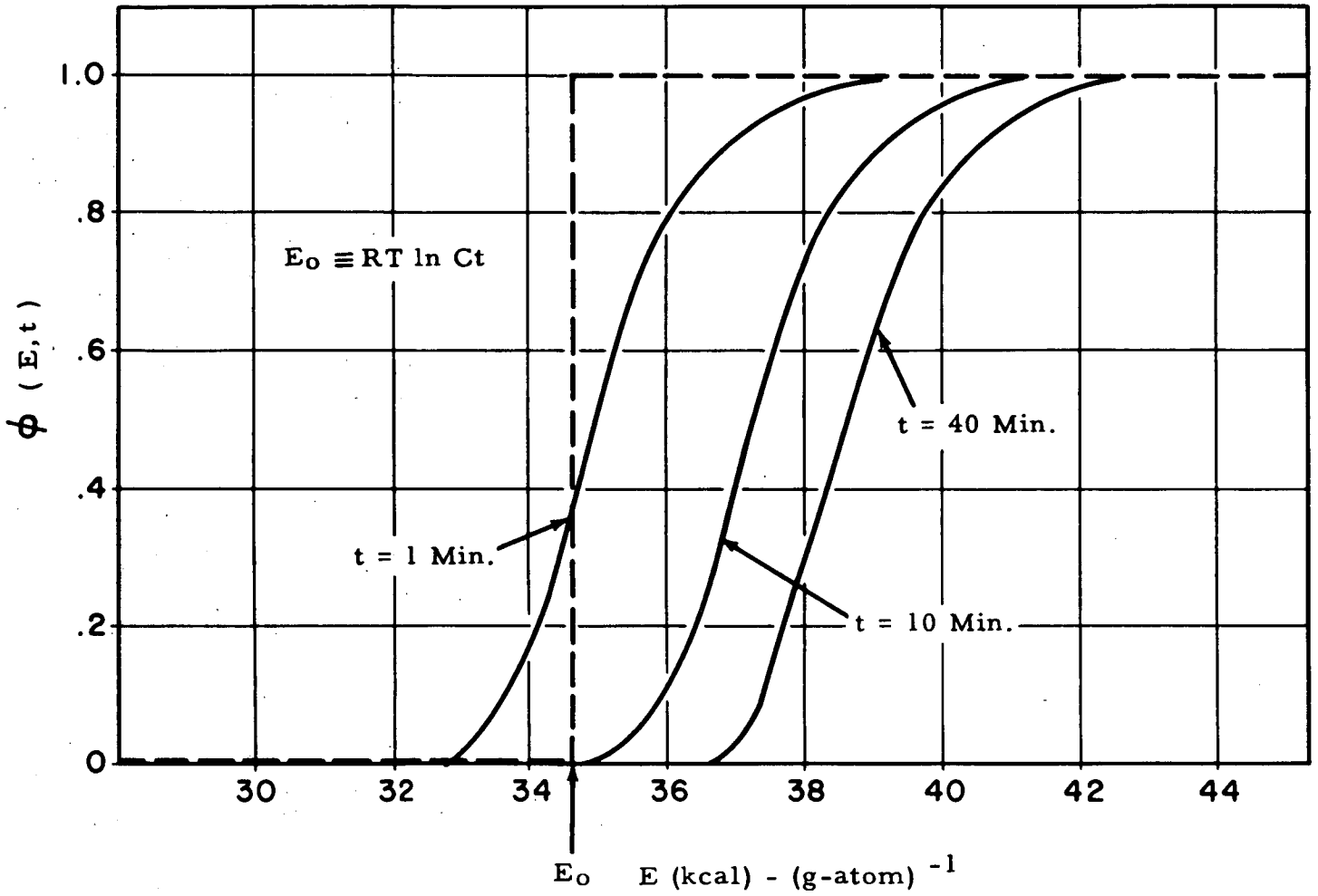

FIGURE 9

ϕ(E, t) vs E

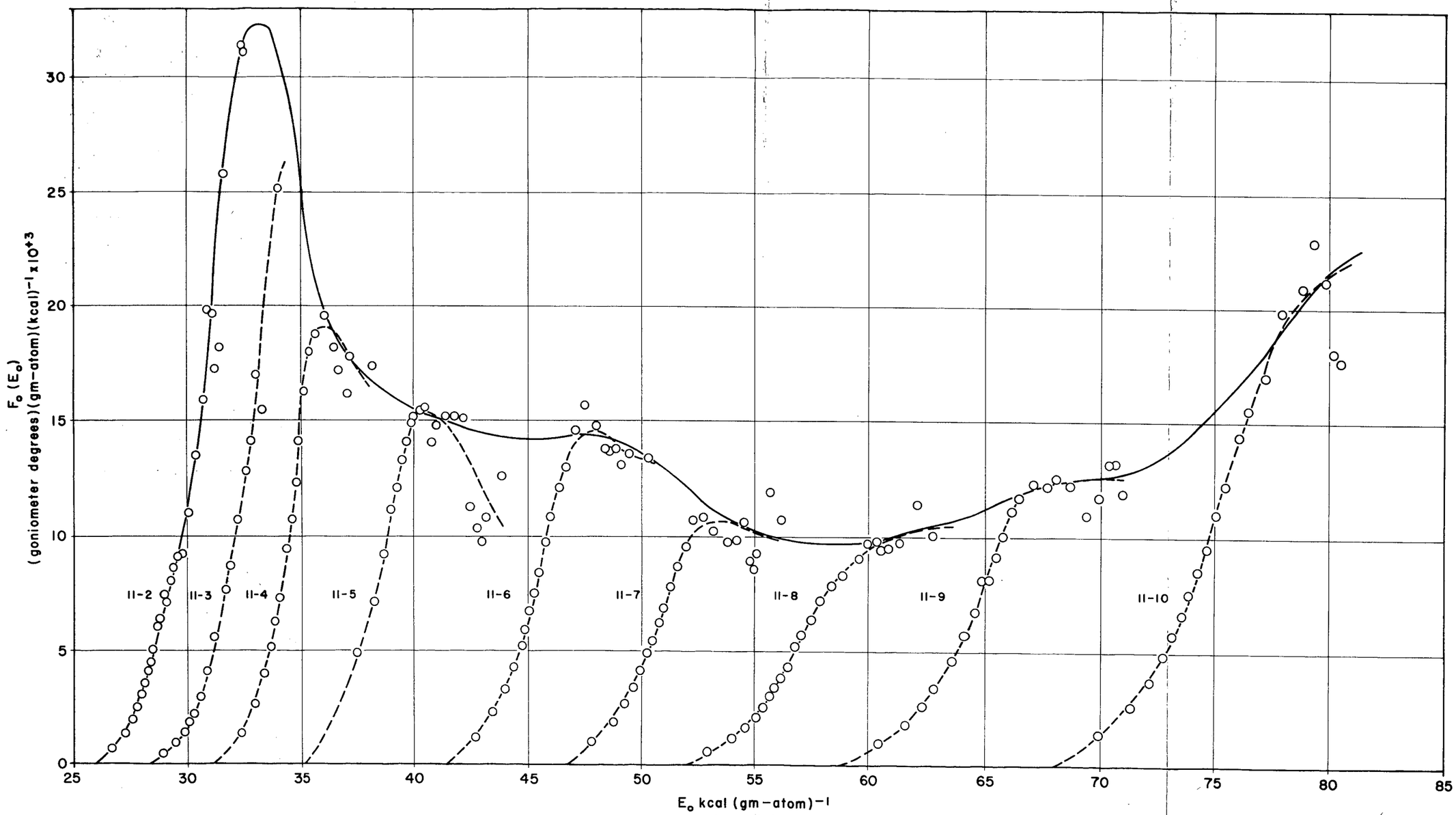

FIGURE 10

ACTIVATION ENERGY SPECTRUM OF IRRADIATED GRAPHITE

AEC-GE RICHLAND, WASH.

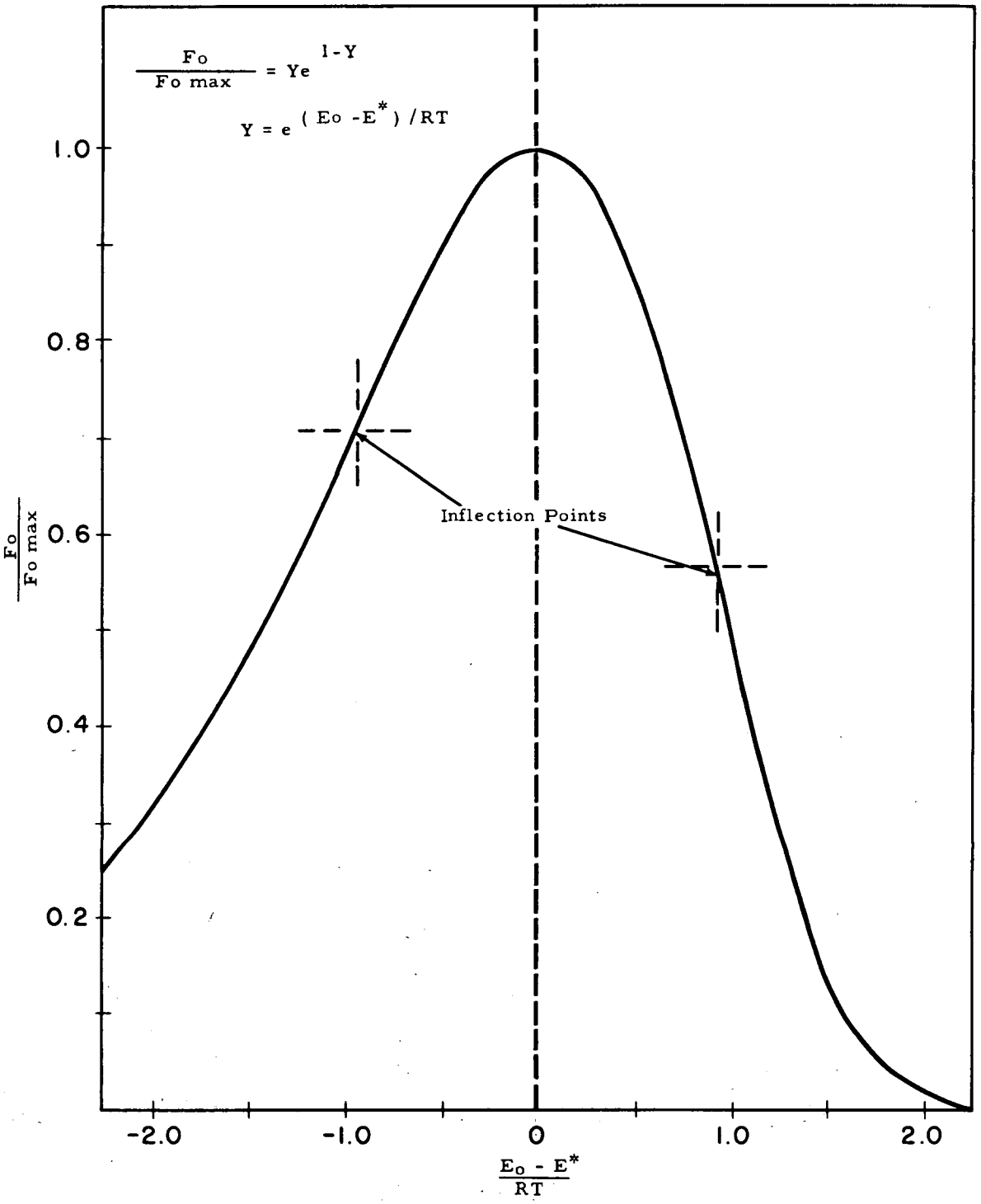

FIGURE 11

EFFECT OF MATHEMATICAL APPROXIMATION TO ϕ

AEC-GE RICHLAND, WN.

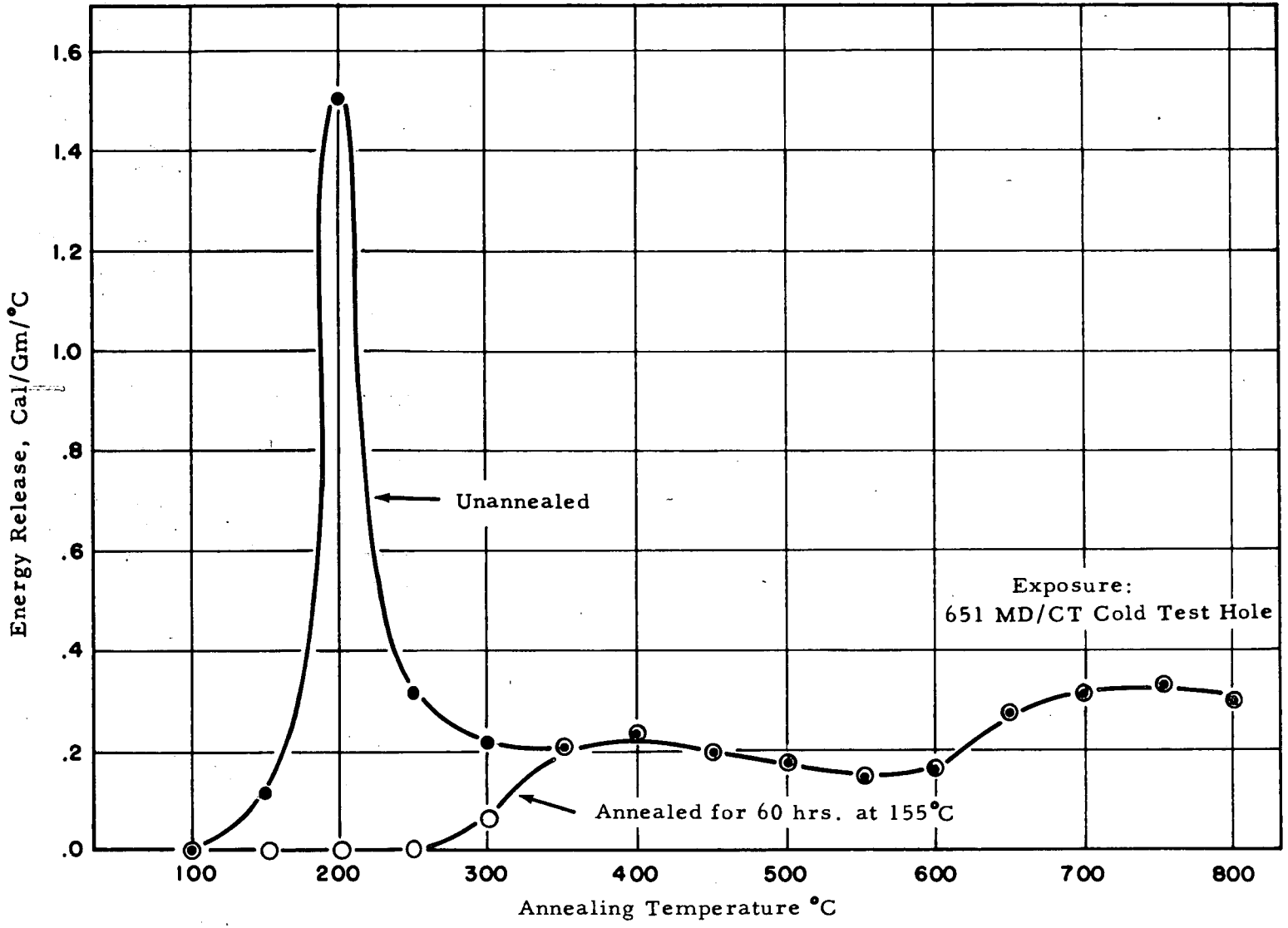

FIGURE 12

STORED ENERGY RELEASE SPECTRA COMPARISON OF ANNEALED AND UNANNEALED SAMPLES

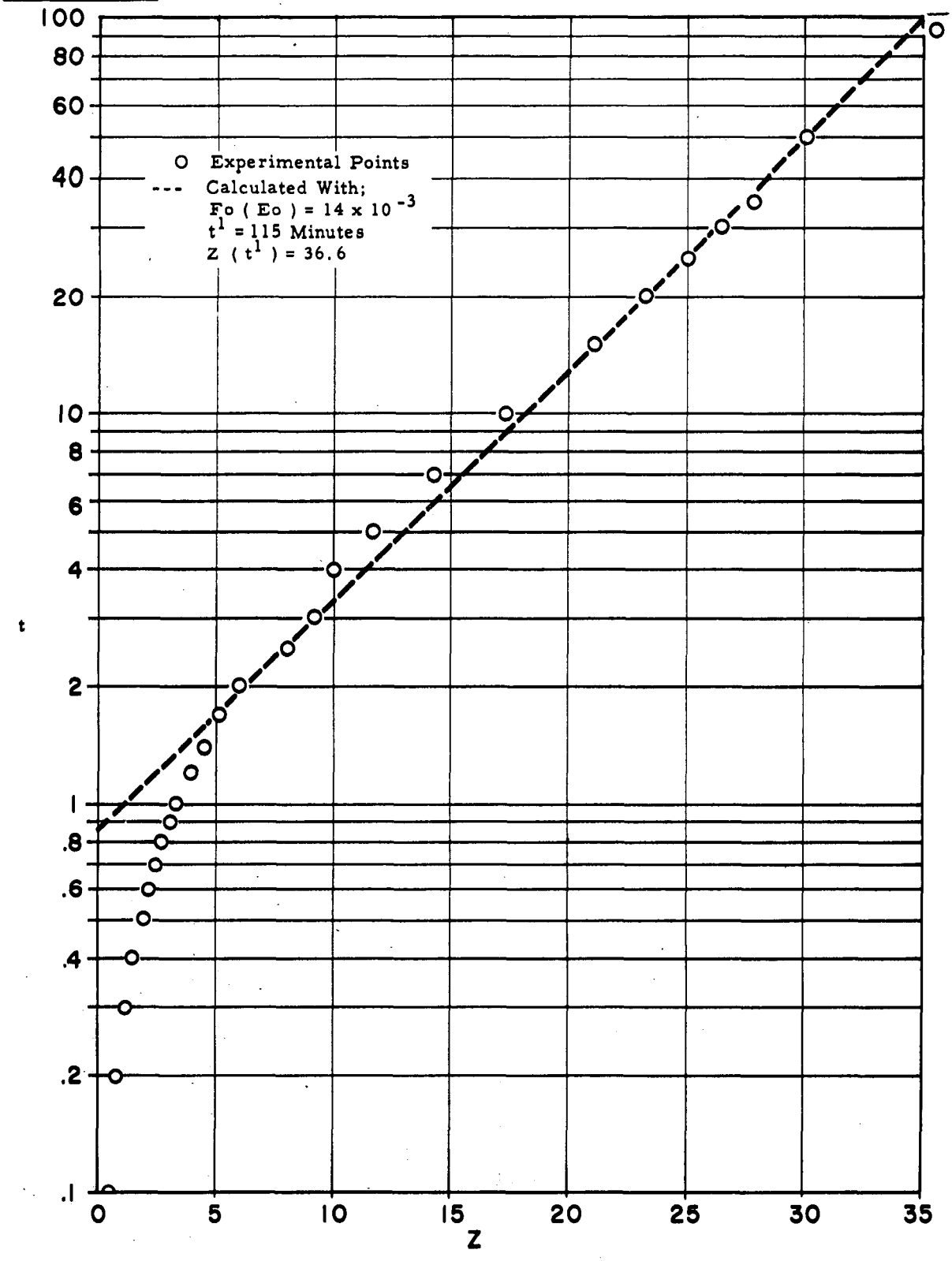

FIGURE 13 OBSERVED AND CALCULATED VALUES OF Z - RUN 11-6

AEC-GE RICHLAND, WN.

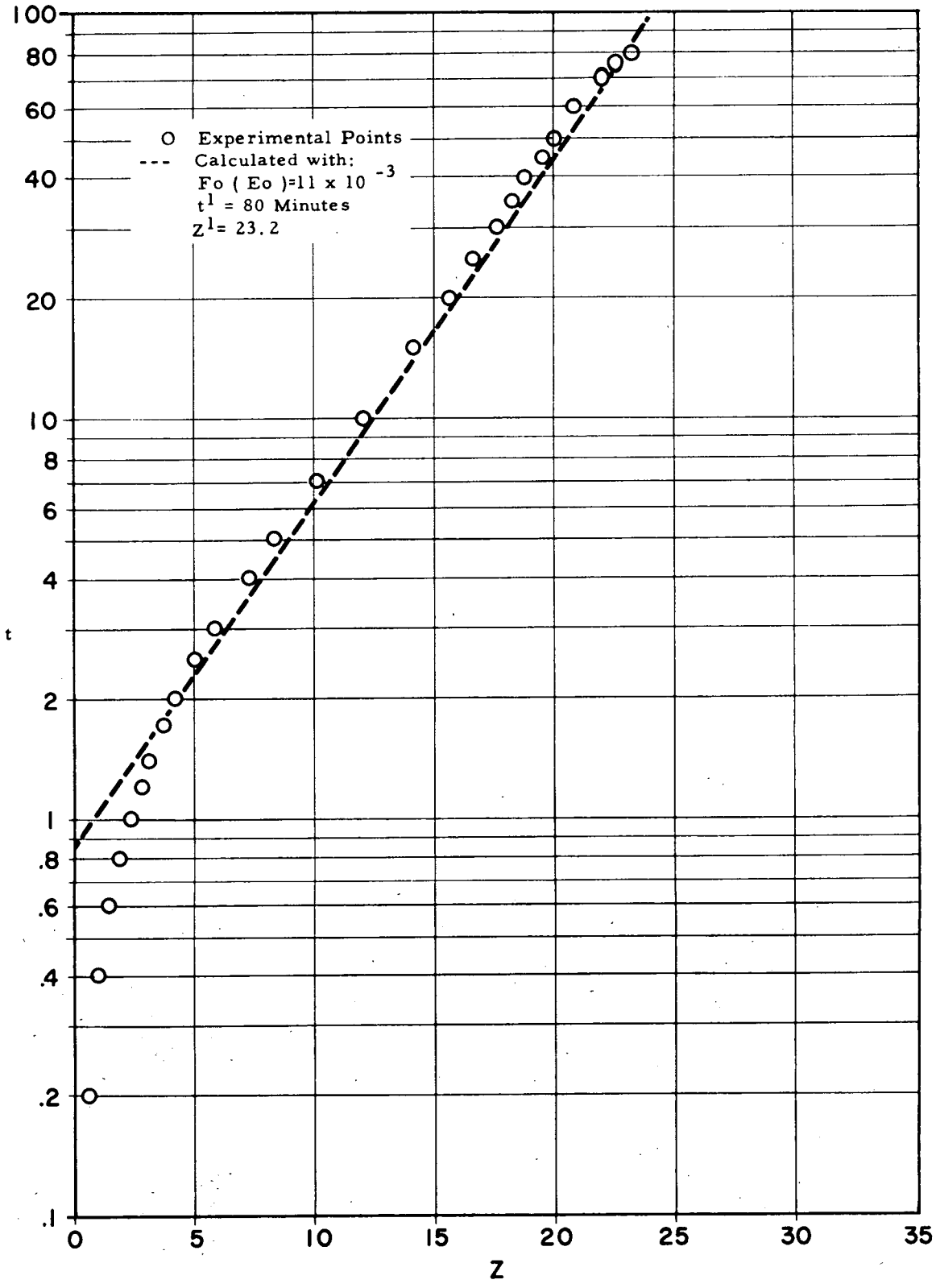

FIGURE 14

OBSERVED AND CALCULATED VALUES OF Z - RUN 11-7 UNCLASSIFIED

43

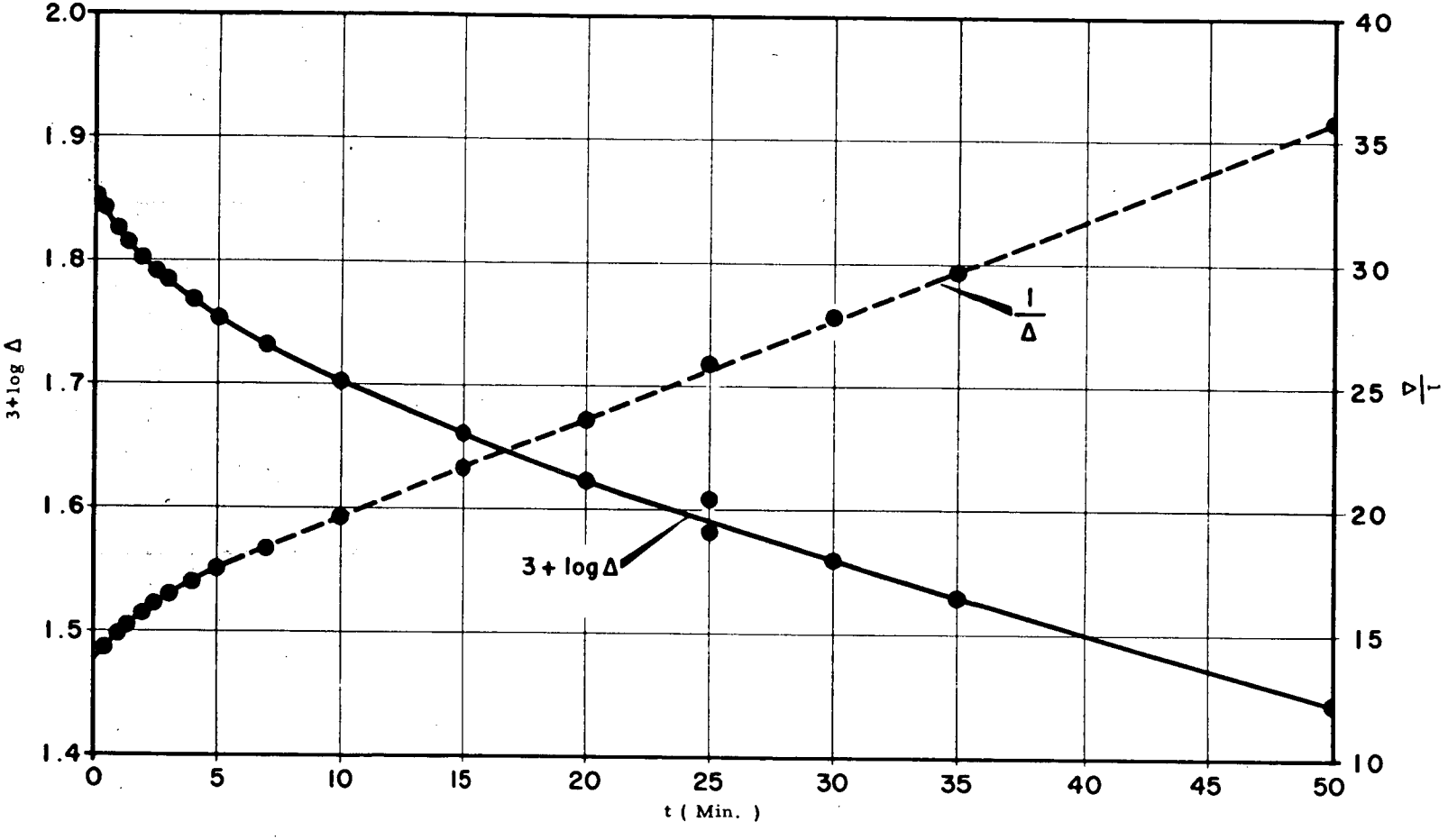

FIGURE 15
FIRST AND SECOND ORDER RATE PLOTS - RUN 11-2

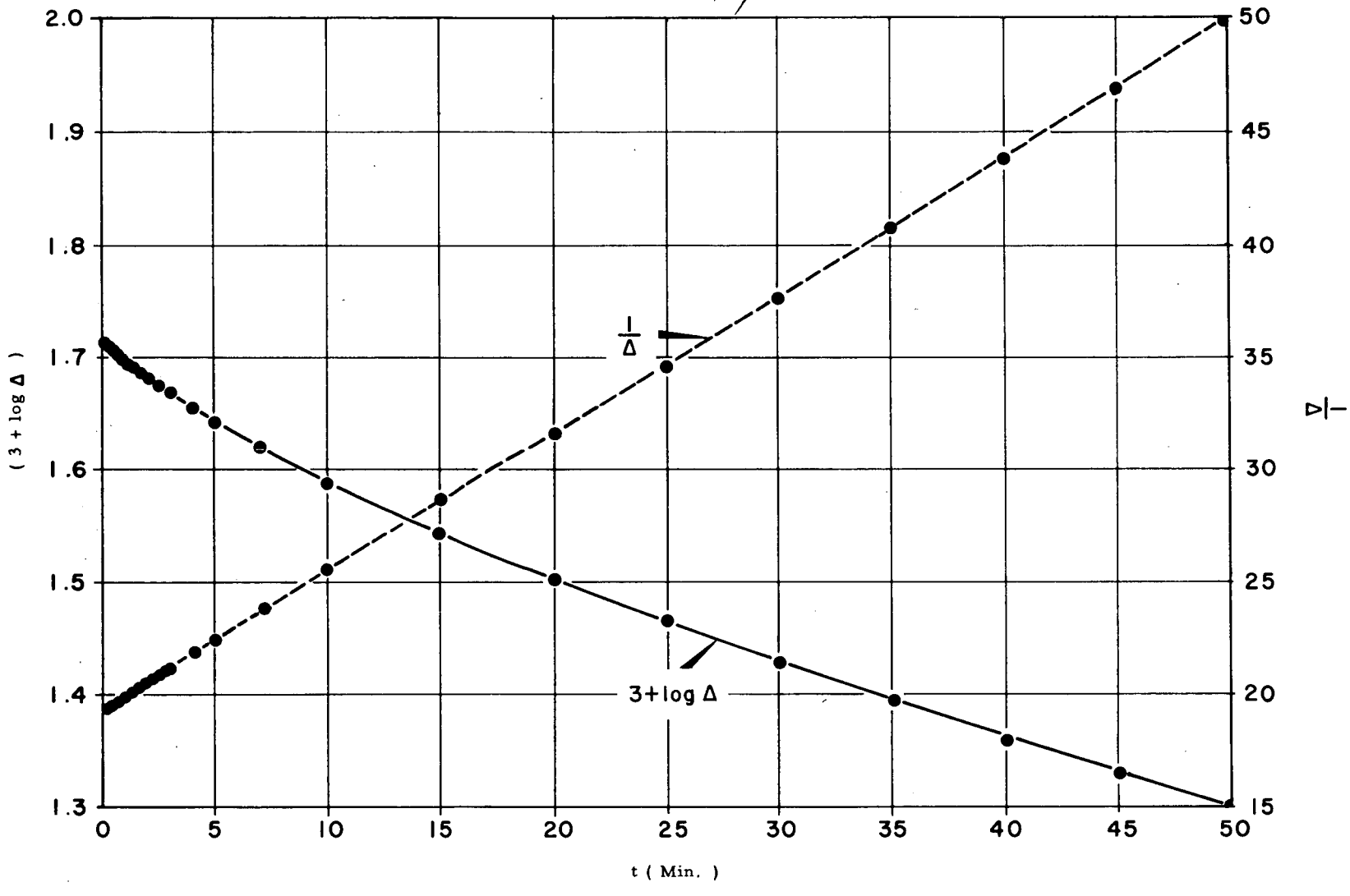

FIGURE 16
FIRST AND SECOND ORDER RATE PLOTS RUN 11-3

TABLE I

EXPERIMENTAL DETAILS

Sample 11

Run	T_A °C	Goniometer Setting (2 θ) during Anneal	Reflection Peak (2 θ) Post-anneal at T_A	Reflection Peak (2 θ) Post-anneal at 25°C
11-1	99	25.67	25.51	25.53
11-2	124	25.61	25.54	25.59
11-3	150	25.64	25.57	25.64
11-4	200	25.69	25.62	25.73
11-5	275	25.69	25.65	25.82
11-6	349	25.74	25.67	25.91
11-7	425	25.76	25.68	25.96
11-8	500	25.80	25.72	26.04
11-9	628	25.76	25.70	26.08
11-10	749	25.77	25.70	26.23

TABLE II

Run 11-2 T_A 125°C			Run 11-3 T_A 150°C			Run 11-4 T_A 200°C		
t (min)	$\Delta(t)\times10^3$	$-\frac{d\Delta(t)}{dt}\times10^3$	t (min)	$\Delta(t)\times10^3$	$-\frac{d\Delta(t)}{dt}\times10^3$	t (min)	$\Delta(t)\times10^3$	$-\frac{d\Delta(t)}{dt}\times10^3$
.1	71.5	5.68	.2	51.7	2.10	.2	81.9	6.68
.2	70.8	5.43	.4	51.2	2.06	.3	81.1	
.3	70.3	5.33	.6	50.7	2.01	.4	80.3	6.41
.4	69.8	5.03	.8	50.4	1.98	.5	79.8	
.5	69.3	4.93	1.0	50.1	1.89	.6	79.3	6.30
.6	68.8	4.76	1.2	49.9		.7	78.8	
.7	68.3	4.65	1.4	49.4	1.78	.8	78.0	6.07
.8	68.0	4.45	1.7	48.8		.9	77.5	
.9	67.5	4.38	2.0	48.3	1.72	1.0	77.0	5.90
1.0	67.0	4.19	2.5	47.5		1.2	75.7	5.69
1.2	66.0	3.99	3	46.7	1.56	1.4	74.5	
1.4	65.3	3.60	4	45.2		1.7	72.9	5.18
1.7	64.3	3.47	5	44.1	1.27	2.0	71.4	5.04
2.0	63.3	2.79	7	41.5	1.04	2.5	69.1	4.62
2.5	62.0	2.53	10	38.9	0.90	3	66.8	4.41
3	60.5	2.26	15	34.9	0.72	4	62.7	3.83
4	58.5	1.80	20	31.5	0.59	5	59.2	3.38
5	57.0	1.46	25	29.1	0.57	7	53.3	2.52
7	54.3	1.24	30	26.8		10	47.2	1.84
10	51.0	1.07	35	24.7	0.37	15	39.8	1.14
15	46.3	.84	40	22.8		20	35.2	0.81
20	42.3	.79	45	21.5		25	31.9	0.60
25	38.5	.62	50	20.0		30	29.1	0.51
30	36.0	.46	60	16.3		35	26.3	0.48
35	33.8	.41	70	12.3		50	19.1	0.41
50	28.0	.41	75	10.5		70	11.2	0.35
136	9.5	.18	80	8.7	0.26	100	3.8	0.16
150	6.5	.16	95		0.15	120	1.8	.03
			100	4.2				

TABLE II (contd.)

Run 11-5 T_A 275°C			Run 11-6 T_A 350°C			Run 11-7 T_A 425°C		
t (min)	$\Delta(t)\times10^3$	$-\frac{d\Delta(t)}{dt}\times10^3$	t (min)	$\Delta(t)\times10^3$	$-\frac{d\Delta(t)}{dt}\times10^3$	t (min)	$\Delta(t)\times10^3$	$-\frac{d\Delta(t)}{dt}\times10^3$
.2	88.6	26.88	.2	77.9	7.60	.2	68.5	6.71
.4	83.9	19.32	.4	76.3	7.16	.4	67.4	6.45
.6	80.3	16.73	.6	74.8	6.87	.6	66.0	6.18
.8	77.1	15.07	.8	73.7	6.65	.8	64.9	5.92
1.0	74.4	13.20	1.0	72.4	6.39	1.0	63.5	5.74
1.2	72.0	12.07	1.2	71.1	6.13	1.2	62.4	5.61
1.4	69.7	10.95	1.4	69.8	5.94	1.4	61.6	5.35
1.7	66.5	9.57	1.7	68.3	5.48	1.7	60.0	5.09
2.0	64.0	8.27	2.0	66.6	5.21	2.0	58.6	4.75
2.5	60.6	6.77	2.5	62.0	4.82	2.5	56.1	4.31
3	57.2	5.67	3	59.6	4.45	3	54.2	4.01
4	52.5	3.82	4	57.9	3.74	4	50.3	3.30
5	49.1	3.23	5	54.2	3.22	5	47.3	2.96
7	43.6	2.37	7	48.5	2.58	7	42.4	2.14
10	37.6	1.65	10	42.0	1.95	10	37.1	1.42
15	31.0	1.10	15	33.7	1.22	15	31.4	0.89
20	26.8	0.61	20	28.9	0.86	20	27.2	0.68
25	24.2	0.45	25	25.0	0.68	25	24.5	0.59
30	22.1	0.35	30	22.0	0.57	30	21.7	0.41
35	20.6	0.31	35	19.1	0.47	35	20.1	0.34
70	11.3	0.20	50	14.1	0.34	40	18.7	0.32
100	6.4	0.09	93	2.2	0.17	60	12.9	0.28
						85	5.2	0.17

48

TABLE II (contd.)

Run 11-8 T_A 500°C			Run 11-9 T_A 628°C			Run 11-10 T_A 749°C		
t (min)	$\Delta(t)\times10^3$	$-\frac{d\Delta(t)}{dt}\times10^3$	t (min)	$\Delta(t)\times10^3$	$-\frac{d\Delta(t)}{dt}\times10^3$	t (min)	$\Delta(t)\times10^3$	$-\frac{d\Delta(t)}{dt}\times10^3$
.2	65.9	4.57	.1	102.6	17.40	.2	138.5	13.86
.4	64.9	4.40	.2	100.4	16.47	.4	135.7	13.15
.6	64.1	4.22	.3	99.3	15.54	.6	132.9	12.61
.8	63.3	4.07	.4	97.4	15.11	.8	130.8	12.16
1.0	62.6	3.87	.6	94.9	13.82	1.0	128.3	11.57
1.2	61.8	3.79	.8	91.6	12.85	1.2	126.2	11.19
1.4	61.0	3.71	1.0	89.4	12.06	1.4	124.0	10.83
1.7	59.7	3.45	1.2	87.2	11.41	1.7	120.3	10.15
2.0	58.7	3.32	1.4	85.0	10.42	2.0	117.5	9.65
2.5	57.2	3.17	1.7	82.0	9.62	2.5	113.2	8.92
3	55.6	2.91	2.0	79.2	8.93	3	108.6	8.29
4	53.3	2.44	2.5	75.1	7.95	4	100.9	7.33
5	51.0	2.20	3	71.5	6.98	5	93.8	6.32
7	47.1	1.71	4	65.2	5.51	7	83.1	4.93
10	43.0	1.28	5	60.5	4.36	10	68.9	4.02
15	37.9	0.92	7	52.8	3.21	15	52.9	2.83
20	33.2	0.74	10	44.8	2.19	20	40.3	2.33
25	30.1	0.60	15	36.0	1.30	25	29.2	1.72
30	27.3	0.48	20	30.3	1.10	30	22.8	1.16
35	25.0	0.42	25	25.0	0.94	35	17.2	0.97
50	20.1	0.30	30	20.4	0.79	50	5.8	0.45
83	11.8	0.21	35	16.8	0.61	70	3.4	0.11
127	4.4	0.12	50	10.7	0.29			
			87	4.4	0.09			